Small-size MEMS Accelerometer Encapsulated in Vacuum Using Sigma-Delta Modulation

Vasco Lima*†, Jorge Cabral*†, Burkhard Kuhlmann‡, João Gaspar† and Luis A. Rocha*†
*Industrial Electronics Department, University of Minho, Guimarães, Portugal
†Micro and Nano Fabrication Department, International Iberian Nanotechnology Laboratory (INL), Braga, Portugal
‡Automotive Electronics, Robert Bosch GmbH, Reutlingen, Germany

***Abstract* – A vacuum encapsulated MEMS accelerometer using Sigma-Delta modulation is here presented. Three different modulation orders (second, third, and fourth) were implemented in a field-programable gate array (FPGA), enabling flexibility for tuning the loop parameters in real-time. Three devices were measured, and the results are in good agreement with simulations performed in Simulink. A noise figure of 123 µg/√Hz for a bandwidth of 400 Hz and a range of at least ±1 g was experimentally measured. A figure of merit considering device size and bandwidth is proposed, highlighting the relevance of the results for the current state of the art.**

Keywords - MEMS, accelerometer, vacuum, Sigma-Delta

I. Introduction

Vacuum encapsulation of MEMS accelerometers can be advantageous since it intrinsically decreases the thermal-mechanical Brownian noise and it enables integration in a single common silicon substrate with other MEMS sensors that require vacuum operation, such as gyroscopes, resonators, and magnetometers. This type of sensor integration can lead to size reduction, as well as fabrication and packaging cost decrease, potentially enabling new applications [1]. However, the low damping required for MEMS gyroscopes and resonators based on the Coriolis force makes the accelerometer more challenging to operate, causing undesirable high settling times.

Electromechanical Sigma-Delta modulators can provide the electrical damping necessary for low-pressure accelerometers while providing high resolution and linearity, and low thermal dependency and susceptibility to process variations, representing one of the most attractive architectures for achieving high-performance MEMS inertial sensors [2]–[4]. Additionally, including the MEMS sensor element into a Sigma-Delta modulating loop enables the realization of a digital sensor interface.

Vacuum encapsulated MEMS accelerometers using Sigma-Delta modulation can be found in the literature, but all present a common issue: large proof-mass [1], [5]–[7]. A big proof-mass has several drawbacks, such as reduced full-scale, added complexity of the manufacturing process, and integration limitations, ultimately leading to cost increase [8].

In this work, a small-size and low-pressure MEMS accelerometer operated in a closed-loop Sigma-Delta modulator implemented in an FPGA is presented. Experimental and simulation data are compared, showing a good agreement. The results are compared with similar devices presented in the literature, and a figure of merit is proposed, highlighting the obtained results.

II. The Electromechanical Sigma-Delta Modulator

An electromechanical Sigma-Delta modulator is a system that includes several different domains. The proposed architecture (presented in Fig. 1) consists of five parts: a) the MEMS sensor, that transforms the physical input acceleration into an electrical capacity change; b) the readout circuit, which converts the change in capacity into a proportional voltage, and later digitalizes that voltage; c) the phase-lag compensator, to compensate the phase shift introduced by the sensor element; d) the Sigma-Delta loop filter, which provides the noise shaping; e) the one-bit DAC, responsible for providing the electrostatic force feedback to the MEMS element.

It is essential to notice that all digital blocks were implemented using floating-point operations for reduced quantization noise.

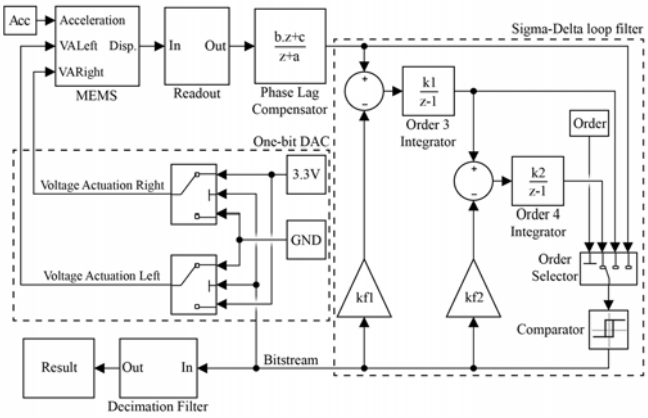

Fig. 1. Proposed architecture for the electromechanical Sigma-Delta modulator.

A. The MEMS sensing element

Three in-plane single-axis capacitive MEMS accelerometers were fabricated and encapsulated with a cavity pressure of 140 Pa using a standard Bosch silicon surface micromachining process. The fabricated devices can be seen in Fig. 2.

On the sensing direction, their behavior can be represented by a mass-spring-damper system, whose displacement x can be expressed as:

$$x = \frac{1}{s^2 + \frac{\omega_0}{Q}s + \omega_0^2} \times a_{in}, \qquad (1)$$

where $\omega_0 = \sqrt{k/m}$ and $Q = \sqrt{mk}/b$ are the resonant frequency and the quality factor, respectively, a_{in} is the input acceleration, m is the mass of the proof mass, k is the

978-1-7281-2983-9/20/$31.00 ©2020 IEEE

stiffness constant of the mechanical springs, and b is the damping coefficient.

The devices have a size of approximately 450×450 μm^2, with a suspended mass (m) of 2.83 μg (364×400 μm^2), a nominal sensing capacity (C_{S0}) of 246 fF, a nominal actuation capacity (C_{A0}) of 148 fF, and a gap at rest (d_0) of 1.6 μm. The elastic coefficient of the mechanical springs (k) is 0.75 N/m, resulting in a resonant frequency (ω_0) of 2591 Hz and a quality factor (Q) of 58.6.

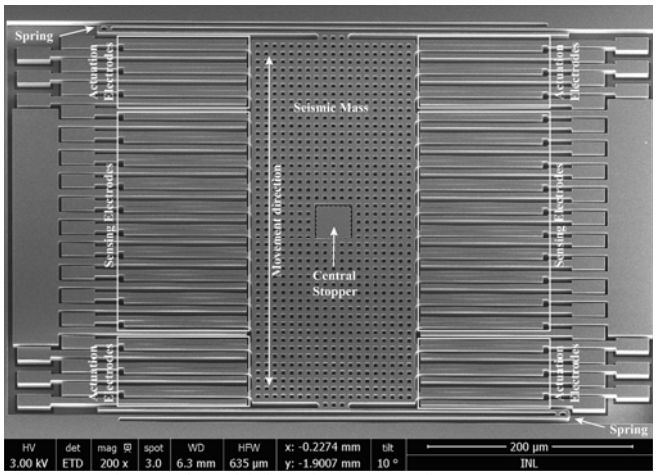

Fig. 2. SEM image of one fabricated MEMS accelerometer.

B. The readout circuit

The first element of the readout circuit is a capacity to voltage (C/V) converter. An in-house designed application-specific integrated circuit (ASIC), based on switch capacitors, that is capable of converting the changes in the capacitance of the accelerometer into a DC voltage, was used. [9] The output voltage of the C/V converter is digitalized using a commercial off-the-shelf (COTS) 16-bit analog to digital converter (ADC) capable of an acquisition frequency of 40 MHz.

An infinite impulse response (IIR) low-pass filter was digitally implemented in FPGA and included as part of the readout system. The filter was implemented using three second-order stages, realizing a sixth-order IIR low-pass filter, and its cutoff frequency is 80 kHz. The block diagram of a second-order section of the implemented filter can be seen in Fig. 3.

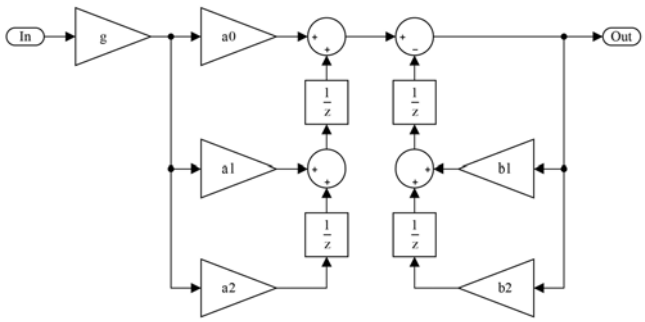

Fig. 3. Block diagram of a second-order section of the implemented IIR low-pass filter.

C. The phase-lag compensator

The phase lag compensator aims to minimize the phase delay introduced by the MEMS device and readout circuit. The compensator was digitally implemented in FPGA and is based on the approach proposed by William Messner in [10]. Its discrete-time transfer function is

$$H_C(z) = \frac{bz + c}{z + a}, \tag{2}$$

which is derived from the continuous-time transfer function

$$H_C(s) = \frac{s + z}{s + p}. \tag{3}$$

To calculate parameters z and p, one can use

$$z = \omega_m \frac{1 - \sin(\phi_m)}{\cos(\phi_m)} \tag{4}$$

$$p = \omega_m \frac{1 + \sin(\phi_m)}{\cos(\phi_m)}, \tag{5}$$

where ω_m is the frequency of maximum phase lead and ϕ_m is the phase lead at that frequency.

D. The Sigma-Delta loop filter

The Sigma-Delta modulator, depicted in Fig. 1, was digitally implemented in FPGA, enabling a fast and accurate tuning of the loop parameters, which is typically performed by simulation [3]. However, the flexibility of the system allows an experimental fine-tuning at the final trim of the devices. This aims to achieve stability of the loop, more difficult for low-damping devices, and to improve the system's performance.

The proposed architecture is able to realize a second, third, or fourth-order electromechanical Sigma-Delta modulator, and feedback and feedforward gains for each modulation order were implemented (kf1, k1, kf2, and k2). The feedback bitstream has a sampling frequency of 500 kHz, and the output of the system is handled by the decimation filter, which has a cutoff frequency of 400 Hz, and it outputs a 32-bit result with a decimation ratio of 500.

E. The one-bit DAC

The force feedback is handled by the electrostatic force of the parallel-plate actuation electrodes, which can be expressed as:

$$F_{elec} = \frac{C_{A0} d_0 V_f^{\,2}}{2(d_0 + x)^2}, \tag{6}$$

where V_f is the actuation voltage. For this work, the force feedback voltage used was 3.3V, implemented as a one-bit digital to analog converter (DAC).

III. Experimental Results

A mechanical characterization of the three devices was performed, and the results were compared with the theoretical values (Table I). For all devices, the experimental values are within a 5% deviation of the theoretical expectation. Moreover, the differences between devices are even smaller, validating a good fabrication process tolerance. The quality factor is the parameter with the most significant deviations, due to variations in the encapsulation pressure.

The performance of the system was evaluated in open-loop (where the system's output is the voltage of the C/V converter) and closed-loop, with second, third, and fourth-order electromechanical Sigma-Delta modulators. To assess the response for different accelerations, the samples were coupled to a precision motor and mechanically excited through the gravitational acceleration (Fig. 4 shows the experimental setup), attaining an experimental measurement range of ± 1g. To achieve loop stability and to improve the system's performance, the gains were manually adjusted through experimental data. The phase lag compensator was tuned for a phase lead of 82 ° at 42750 Hz, and kf1, k1, kf2, and k2 were adjusted to 27, 0.3, 87, and 0.1, respectively.

In Table II, the experimental sensitivity and non-linearity are presented. The sensitivity increased drastically from open-loop to closed-loop by a factor of over 900000, improving the overall system performance. These results are corroborated by the simulation model. Even though the experimental non-linearity of all devices is below 0.76% for every modulation order, below the desired 1%, the simulated values are significantly lower. These differences are attributed to misalignments on the experimental setup, which can occur on the X, Y and Z axis, and on several parts composing the setup (e.g., the MEMS is manually glued to the carrier, the socket is soldered to the printed circuit board (PCB) by hand, the PCB is coupled to the precision motor by hand, …). These misalignments lead to increased non-linearities due to measurement procedures and not because of the devices themselves.

The noise level of the system was evaluated through Allan variance measurements. From Fig. 5, one can see that the results for each modulation order are similar between devices, resulting in noise figures of 7.3 mg/√Hz for open-loop configuration and 594 µg/√Hz, 123 µg/√Hz, and 125 µg/√Hz for second, third, and fourth-order modulators, respectively. Additionally, third and fourth-order modulators yield approximately the same results. The experimental results are in close agreement with the simulation model, and the high modulation order and low-frequency differences can be explained by the simplified readout circuit model, which was implemented as a C/V gain with white noise only.

The overall better results achieved by higher modulation orders are in accordance with the fundamental theory of Sigma-Delta modulation.

Table I. Theoretical and experimental data of the mechanical characterization.

	Theor. Value	Dev. 1	Dev. 2	Dev. 3
Pull-in voltage (V)	1.962	1.893	1.892	1.888
Pull-in voltage error (%)	-	3.5	3.6	3.8
Resonant frequency (Hz)	2591	2535	2537	2536
Resonant frequency error (%)	-	2.2	2.1	2.1
Quality factor	58.6	58.3	56.0	58.6
Quality factor error (%)	-	0.5	4.4	0.0

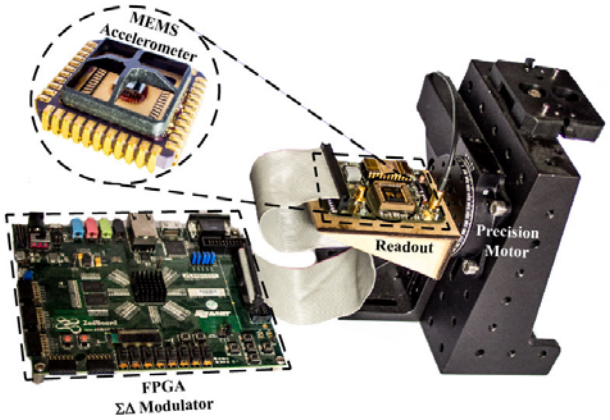

Fig. 4. Experimental setup.

Table II. Simulated and experimental sensitivity and non-linearity results.

		Sim.	Dev. 1	Dev. 2	Dev. 3
Sensitivity (Bit/g)	**Open-loop**	6.75	6.74	6.74	6.76
	Order 2	26.76	26.76	26.71	26.71
	Order 3	26.34	26.56	26.60	26.55
	Order 4	26.34	26.56	26.61	26.54
Non-linearity (%)	**Open-loop**	0.03	0.62	0.46	0.48
	Order 2	0.10	0.65	0.63	0.54
	Order 3	0.05	0.43	0.67	0.44
	Order 4	0.05	0.67	0.76	0.38

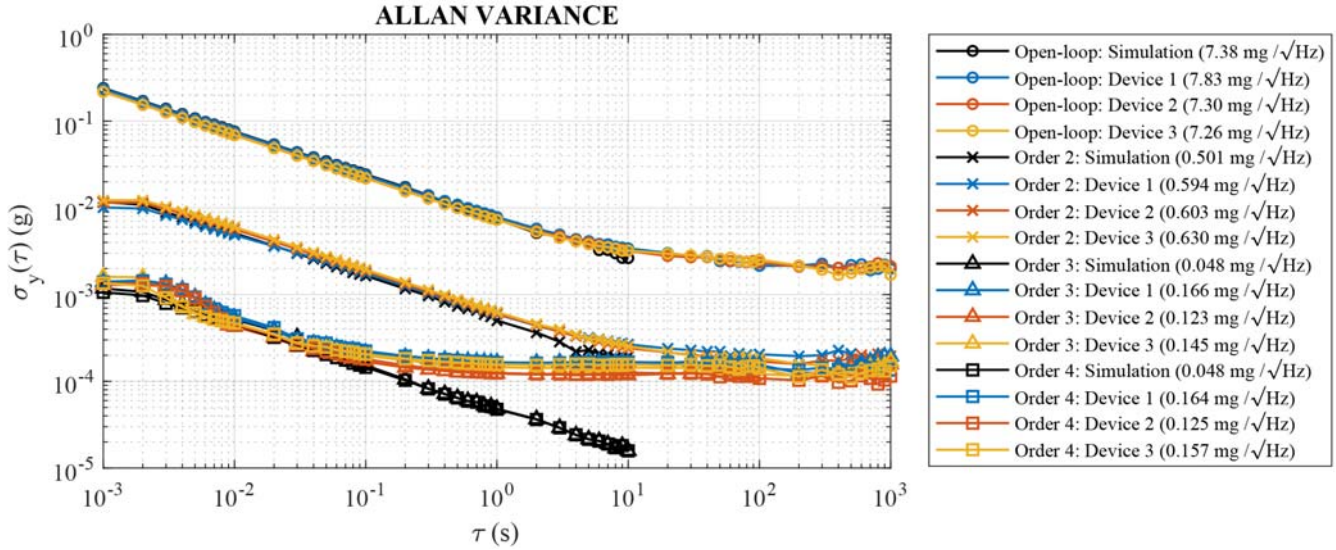

Fig. 5. Experimentally measured Allan variance.

To compare the obtained results with the literature, two figures of merit (FOM) are proposed, relating the achieved noise level with the bandwidth and size of the sensor (Table III). These characteristics were chosen since device size and bandwidth are closely related to the noise level. On the one hand, a device with a large proof-mass intrinsically has lower thermal-mechanical Brownian noise, improving its overall noise performance. Additionally, with a large footprint sensor, larger capacitances are easier to achieve, improving the device sensitivity and consequently the signal-to-noise ratio. On the other hand, a lower bandwidth signal allows for more restricted filtering and higher integration times, which also leads to the realization of lower noise levels.

The proposed FOMs (FOM1 = Vol.Noise/BW and FOM2 = Mass.Noise/BW) multiply the noise level achieved by the device size (either volume of the proof-mass for FOM1 or mass of the proof-mass for FOM2) and divide the result by the achieved bandwidth. Once bigger size and lower bandwidth realize lower noise, a smaller result (in both FOM) translates to better relative performance.

According to both figures of merit, the performance of the presented accelerometer stands out from the ones found in the literature.

Table III. Comparison between the literature and this work.

	[5] Dong (2011)	**[1] Chen (2014)**	**[6] Li (2018)**	**[7] Wang (2018)**	**This work**
Seismic mass volume (mm^3)	1.50	1.40	-	-	0.0028
Seismic mass (nKg)	-	1620	620	14300	2.83
Noise figure (µg/√Hz)	17	12	4.8	2.0	1230
Bandwidth (Hz)	300	500	300	300	400
Vol.Noise/BW (mm^3.ng/$Hz^{1.5}$)	8.50	3.36	-	-	0.85
Mass.Noise/BW (nKg.µg/$Hz^{1.5}$)	-	3.89	0.99	9.53	0.87

IV. Conclusions

Small size and vacuum encapsulated capacitive MEMS accelerometers using Sigma-Delta modulation were presented in this paper. Three devices were fabricated and tested. The electromechanical Sigma-Delta modulator architecture was digitally implemented in FPGA, enabling the flexibility of a fast and effective tuning of the parameters for the final trim of the devices.

The best noise figure achieved was 123 µg/√Hz for a bandwidth of 400 Hz and a measurement range of ±1 g. The measured non-linearity is below 0.76 % in all cases. As expected, higher modulation orders can achieve better performance.

Two figures of merit were proposed, relating noise level with device size and bandwidth, highlighting the value proposition of this work.

Acknowledgments

The first author is supported by FCT– Fundação para a Ciência e Tecnologia through the grant PDE/BDE/114563/2016.

Part of this work was developed under "Development and Industrial Validation of a Multimodal Virtual Prototyping for In-Car Design (Product in Touch)" Project, receiving funding from COMPETE agency, PT2020 funding program, under contract No.: POCI-FEDER-033699.

The authors would like to offer special thanks to the author Luis A. Rocha, who, although no longer with us, continues to inspire by his example and dedication to the students and collaborators he served over the course of his career.

References

[1] F. Chen, W. Yuan, H. Chang, I. Zeimpekis, and M. Kraft, "Low noise vacuum MEMS closed-loop accelerometer using sixth-order multi-feedback loops and local resonator sigma delta modulator," in *IEEE 27th International Conference on Micro Electro Mechanical Systems (MEMS)*, 2014, pp. 761–764.

[2] Jiangfeng Wu and L. R. Carley, "Electromechanical ΔΣ modulation with high-Q micromechanical accelerometers and pulse density modulated force feedback," *IEEE Trans. Circuits Syst. I Regul. Pap.*, vol. 53, no. 2, pp. 274–287, Feb. 2006.

[3] R. Wilcock and M. Kraft, "Genetic Algorithm for the Design of Electro-Mechanical Sigma Delta Modulator MEMS Sensors," *Sensors*, vol. 11, no. 12, pp. 9217–9232, Sep. 2011.

[4] Z. Meimei, Q. Haiyang, and Z. Fuqiang, "Comparisons of Feed-Forward and Multiple-Feedback Sigma-Delta Modulators for MEMS Accelerometers," *MATEC Web Conf.*, vol. 56, p. 08003, Apr. 2016.

[5] Y. Dong, P. Zwahlen, A. M. Nguyen, R. Frosio, and F. Rudolf, "Ultra-high precision MEMS accelerometer," in *16th International Solid-State Sensors, Actuators and Microsystems Conference*, 2011, pp. 695–698.

[6] X. Li, J. Hu, and X. Liu, "A High-Performance Digital Interface Circuit for a High-Q Micro-Electromechanical System Accelerometer," *Micromachines*, vol. 9, no. 12, 2018.

[7] Y. H. Wang, L. Yin, D. L. Chen, L. Li, and X. W. Liu, "A method to reduce harmonic distortion of MEMS accelerometer," *Mod. Phys. Lett. B*, vol. 32, no. 21, 2018.

[8] U. Sonmez, H. Kulah, and T. Akin, "A fourth order unconstrained ΔΣ capacitive accelerometer," in *16th International Solid-State Sensors, Actuators and Microsystems Conference*, 2011, no. 1, pp. 707–710.

[9] F. S. Alves, "Auto-calibrated, thermal-compensated MEMS for smart inclinometers," Universidade do Minho, 2017.

[10] W. Messner, "Formulas for asymmetric lead and lag compensators," in *2009 American Control Conference*, 2009, pp. 3769–3774.